Resonant Cavity 4-λ Integrated 4×4 PD-Array for High Optical Alignment Robustness WDM-FSO Communications

Toshimasa Umezawa, Shoichi Takamizawa, Atsushi Matsumoto, *Member, IEEE*, Kouichi Akahane, Naokatsu Yamamoto, Atsushi Kanno, *Senior Member, IEEE*, and Tetsuya Kawanishi, *Fellow, IEEE*

***Abstract*—We present a newly developed resonant cavity 4-λ integrated two-dimensional 4 × 4 photodetector array (2D-PDA) device and its application for a wavelength-division-multiplexing (WDM) free-space optical (FSO) communication. The 2D-PDA enables direct optical coupling to the FSO beam, simplifying the optical alignment process needed for 10 μm single-mode fiber coupling and reducing the need for beam-tracking function. In the WDM-FSO communication demonstration, a four-wavelength beam in free space was successfully received by 4-different cavity length PD pixels in 4 × 4 PDA with crosstalk between each channel. This paper discusses about the fabrication and characteristic of the 2D-PDA device, in addition to the 25 Gbps/λ FSO communication demonstration using the 4 × 4 2D-PDA. Considering the crosstalk, the bit error rate is discussed in the 2-WDM and 3-WDM FSO communication demonstrations at 25 Gbps/λ.**

***Index Terms*—Free space optical communication, high speed, resonant cavity photodetector, two-dimensional photodetector array, wavelength division multiplexing.**

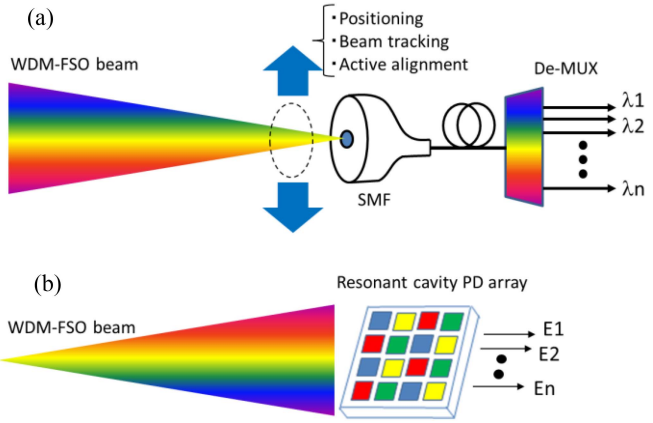

Fig. 1. Schematic illustrations of WDM-FSO receiver, (a) conventional configuration coupled to SMF and AWG, (b) a proposed WDM receiver system using 4-λ integrated PD array.

I. Introduction

RECENTLY, an advanced wireless communication technology on 5G has been expanded to increase the data rate up to 10 Gbps with high demand of internet through mobile communications [1]. Here, usage of high-speed signal in millimeter wave region (28–40 GHz) [2] with that in microwave region (3.6–4.6 GHz) is one of crucial points to increase the total data rate. In next generation of 5G (beyond 5G), usage of unused higher frequency band allocation in D-band (110–170 GHz) [3] is discussed according to a 6G white paper toward 100 Gbps wireless communications [4], however it seems a big challenge to realize the scenario for extreme high data rate in wireless communication fields. In contrast, free space optical (FSO) wireless communication is one of wireless communication technologies based on lightwave instead of radio-wave in 5G–6G communication. Compared to the radio-wave based communications, it will not be difficult to achieve a 100 Gbps data rate per line applying optical fiber communications technologies such as wave division multiplexing (WDM). Here 1 Tbps in single channel was reported by using 32λ-WDM on-off keying [5], and higher data rate of 14 Tbps [6] was also reported using multi-aperture channel system as well. These FSO technology has been mainly studied targeting outdoor communication applications between buildings [7], and between satellites [8]. Moreover, the FSO technology has been recently extended to indoor short range communication applications [9], [10] such as office network and data center network with LiFi system [11].

Fig. 1(a) shows a typical configuration of WDM-FSO system for a fiber to fiber-based connection from a transmitter to a receiver, where a long-range transmission in fiber communication is replaced to free space. FSO beam position is tracked

Manuscript received 28 September 2022; revised 15 December 2022; accepted 16 December 2022. Date of publication 22 December 2022; date of current version 17 April 2023. This work was supported by the R&D of high-speed THz communication based on radio and optical direct conversion under Grant JPJ000254 made with the Ministry of Internal Affairs and Communications of Japan. *(Corresponding author: Toshimasa Umezawa.)*

Toshimasa Umezawa, Atsushi Matsumoto, and Kouichi Akahane are with the Optical Access Technology Laboratory, National Institute of Information and Communications Technology, Koganei-shi 184-8795, Japan (e-mail: toshi_umezawa@nict.go.jp; a-matsumoto@nict.go.jp; akahane@nict.go.jp).

Shoichi Takamizawa is with Fuji Technical Research Corporation, Yokohama-shi 234-0051, Japan (e-mail: sho_takamizawa@ftr.co.jp).

Naokatsu Yamamoto is with Photonic ICT Research Center, National Institute of Information and Communications Technology, Koganei-shi 184-8795, Japan (e-mail: naokatsu@nict.go.jp).

Atsushi Kanno is with the Nagoya Institute of Technology, Nagoya-shi 466-8555, Japan (e-mail: kanno.atsushi@nitech.ac.jp).

Tetsuya Kawanishi is with Waseda University, Shinjuku-ku 169-8050, Japan (e-mail: kawanishi@nict.go.jp).

Color versions of one or more figures in this article are available at https://doi.org/10.1109/JLT.2022.3231344.

Digital Object Identifier 10.1109/JLT.2022.3231344

and adjusted by active alignment function (positioning system) on a receiver [12], [13], and is directly coupled to the optical fiber in a receiver. After the WDM beam passes through the fiber, multiplexed beam is de-multiplexed by an array waveguide grating (AWG) device. Several photoreceivers are aligned and connected to de-multiplexed parallel signals. In particular, the FSO system in case of short-range indoor communications has a great advantage of taking a comparable high data rate to optical fiber communications, because of no optical power attenuation and fluctuation from weather condition and atmospheric turbulence in outdoor environment. A drawback is concerned to a lack of compactness design and a high-cost design due to the beam positioning system. To overcome these issues, simplifying the positioning system, the AWG device and several photodetectors might be ruled out. On the other hand, a resonant cavity photodetector (RC-PD) array is one of good candidate devices to solve the issue in above (see Fig. 1(b)). It has a potential for both enhancing responsivity and filtering specific wavelength. The RC-PDs have been mainly studied for increasing responsivity based on Si [14], SiGe [15], III-V compound [16], [17], [18] materials such as avalanche photodetectors so far. Very few reports focused on filtering specific wavelength for WDM signal detection are presented. In 1991, 1995, Kishino [19] and Selim Unlu [20] proposed a 300 μm large four-PD integrated with different cavity wavelength in 900 nm range targeting WDM fiber communication. The main study in this report was reporting on the theoretical analysis for RC-PD and the proof their design concept regarding the static characteristics and crosstalk between PDs, without high speed WDM-FSO communication demonstration and high optical alignment robustness design.

Recently, we have been studied two-dimensional high speed photodetector array devices and its application for both fiber and FSO communications. It consists of 6 $\times$ 6 matrix structure including 10–30 μm small PD pixels. The PD pixel was carefully arranged to square or triangular shape design in consideration of RF crosstalk affection between the PD pixels, or wirings [21], [22]. Each small PD pixel could work well with 3 dB bandwidth of 11–27 GHz in 10–30 μm PD size. In optical fiber communication application, multi-parallel signals through multi-core fiber directly coupled to the PD array could provide 400–800 Gbps (25–50 Gbps $\times$ 16ch) [23]. A novel phase retrieval coherent receiver was proposed by the PD array as well [24]. Thanks to the large aperture size PD array (0.25 mm), it could be applied for high data rate FSO communication using space diversity [25], and WDM-FSO communications through four color filter in free space [26]. Then high optical alignment robustness could be archived on receiver side.

In this paper, we fabricated and characterized a resonant cavity type large aperture size 4 $\times$ 4 PD array for WDM-FSO communications up to 20–25 Gbps per channel (λ) by using high-speed PD array fabrication technologies in our previous works, assuming large-scale NxN RC-PD array. It plays a role of both high optical alignment robustness and filtering specific wavelengths in WDM beam at the same time. Considering the crosstalk, the bit error rate is discussed in the 2-WDM and 3-WDM FSO communication demonstrations at 25 Gbps/λ.

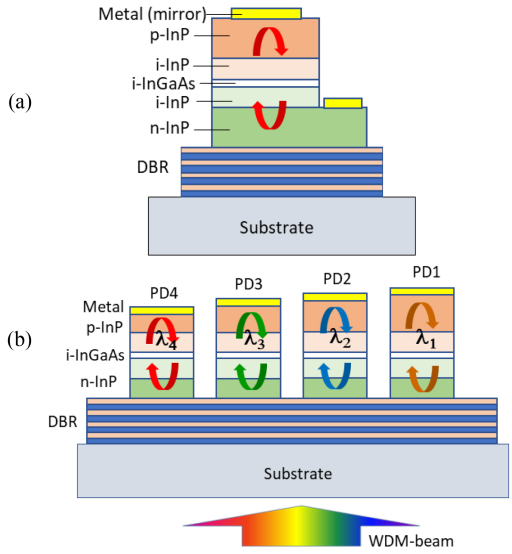

Fig. 2. (a) Schematic cross-sectional-view of a resonant cavity photodetector structure, and (b) 4-λ integrated photodetector array.

II. Design of Resonant Cavity 4 $\times$ 4 -PD Array

A. Responsivity

We designed a resonant cavity 4 $\times$ 4 photodetector array device, which was integrated with four-different cavity length back-illuminated type photodetectors. A quantum efficiency in optical resonant characteristic for 4-WDM filter was calculated by (1) in previous report [18], where R_1, R_2 are reflectivity of front and end mirror, α is absorption coefficient, d is absorption layer thickness, β is propagation constant, L is cavity length, ϕ_1, ϕ_2 are phase in front and end mirrors.

$$\eta = \left\{ \frac{\left(1 + R_2 e^{-\alpha d}\right)}{1 - 2\sqrt{R_1 R_2} e^{-\alpha d} \cos\left(2\beta L + \varphi_1 + \varphi_2\right) + R_1 R_2 e^{-2\alpha d}} \right\} \times \left(1 - R_1\right)\left(1 - e^{-\alpha d}\right) \quad (1)$$

Each PD pixel consisted of p-InP/i-InP//i-InGaAs/i-InP/n-InP on DBR layer on InP substrate (see Fig. 2), and the DBR was designed with multi- stacking thin films based on InGaAlAs and InP material to obtain 75–80% reflectance in C-band as a front mirror. The top Ti/Pt/Au metal plays two roles of both p-ohmic contact metal and reflective end mirror. The reflectance of the end mirror was as low as 75–80%. Under a back-illuminated PD structure, the low reflectance on the Ti end mirror in Ti/Pt/Au top metal or interface affection between a top-semiconductor layer and Ti metal was expected. Under 80% reflectance in front and 75–80% end mirror condition, broadened peak response profile in spectral responsivity was obtained in a short cavity length. It suggested that a crosstalk between four-λ PD pixels would be generated. To make lower crosstalk response profiles less than -10 dB in each channel, the longer cavity length would be designed. When assuming the cavity length of 4 μm including i-InGaAs absorption layer thickness of 0.1 μm, the

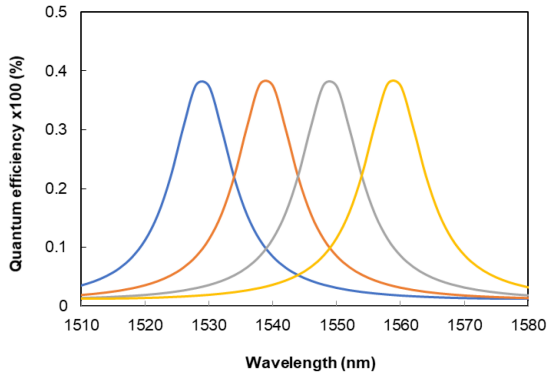

Fig. 3. Simulated spectral responsivity (quantum efficiency) of 4-λ integrated photodetector array.

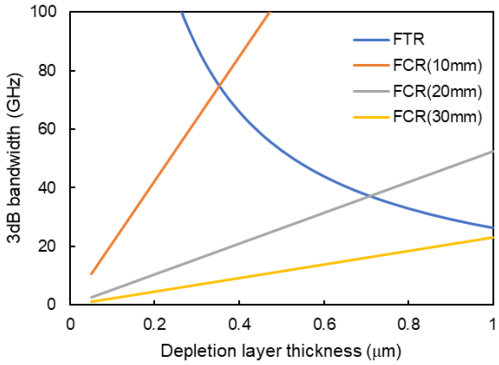

Fig. 4. Calculated 3 dB bandwidth for both carrier travelling time and CR time constant in 10, 20 and 30 μm PD.

resonant spectral responsivity profiles with 25 nm different cavity lengths in each PD were calculated. The WDM response peak was aligned at approximately 10 nm wavelength pitch, and the crosstalk defined by the PD1 peak and PD2 tail responsivity at 1530 nm was designed for −15 dB (see Fig. 3). We recognized that the calculated quantum efficiency of 38% in Fig. 3 would be improved to be 80%, when the reflectivity of end mirror was increased to be 95%.

B. Frequency Response

From viewpoint of enhancing a resonance characteristic in Fabry-Perot mirrors, a thin i-InGaAs layer is required, otherwise crosstalk between channels would be degraded. On the other hand, the thin i-InGaAs layer affects increasing the pn junction capacitance. To prevent from the large junction capacitance issue, the 0.1 μm thin absorption layer was sandwiched by two 0.4 μm thick InP intrinsic spacer layers to reduce the junction capacitance (see i-InP in Fig. 2(a)). Assuming the PD pixel size in range of 10–30 μm, the 3 dB bandwidth was estimated taking the CR time constant and the carrier travelling time into account as shown in Fig. 4. Here the carrier travelling time should be defined by hole drift velocity (5×10^6 sec/cm) in 0.1 μm absorption layer and the i-InP layer. The junction capacitance depends on the total layer thickness of both 0.1 μm absorption layer and i-InP layer. We estimated the 3 dB bandwidth for

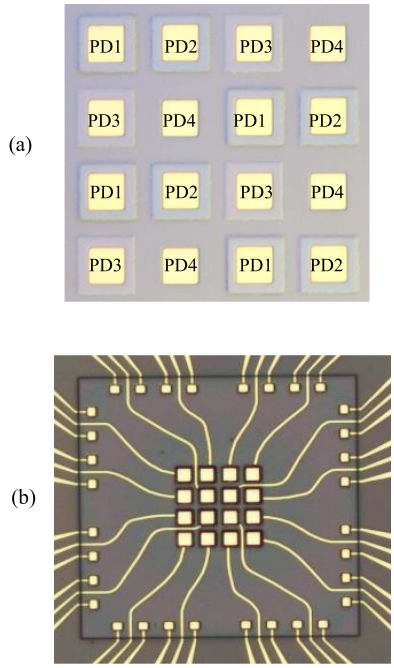

Fig. 5. (a) A photograph after wet etching process in the middle stage to form four resonant cavity high-mesa structures with 25 nm different cavity length, (b) a fabricated 4 × 4 PD array device in the final stage.

10 μm, 20 μm, and 30 μm PD pixel sizes related to the carrier travelling time and CR time constant under various i-InP layer thickness condition, where the absorption layer thickness was fixed to be 0.1 μm (see Fig. 4). For 30 μm PD pixel size for example, the 3 dB bandwidth was mainly dominated by CR time constant (pn junction capacitance) in 1 μm depletion layer region. In 10–20 μm small PD pixel, the 3 dB bandwidth related to carrier travelling time should be considered in addition to the CR time constant. For the 10, 20, and 30 μm PD pixel, the 3 dB bandwidth was estimated as high as 58 GHz, 29 GHz, and 20 GHz respectively.

III. Fabrication and Characteristics

A. Fabrication

We fabricated four different resonant cavity length 4 × 4 photodetector arrays with 30 μm pixel size, where the aperture size is 162 μm × 162 μm. In particular, very careful attention was paid for an etching process to realize 25 nm difference cavity length condition by using wet-chemical etching with very low etching rate (see Fig. 5(a)). Assuming simultaneous irradiation to four-λ PDs in FSO communication, the PD pixel aligned arrangement were considered in the order of "PD1, PD2, PD3, PD4", from left side in first row in 4 × 4 PD array. In second row, it was arranged in order of "PD3, PD4, PD1, PD2". The layout in third and fourth rows was arranged to the same as that in first and second rows again. The layout attributes not only 4-WDM beam simultaneous detection, but also allowing the high optical alignment robustness in FSO, when the FSO beam hit any four PDs in 4 × 4 PD array simultaneously. After

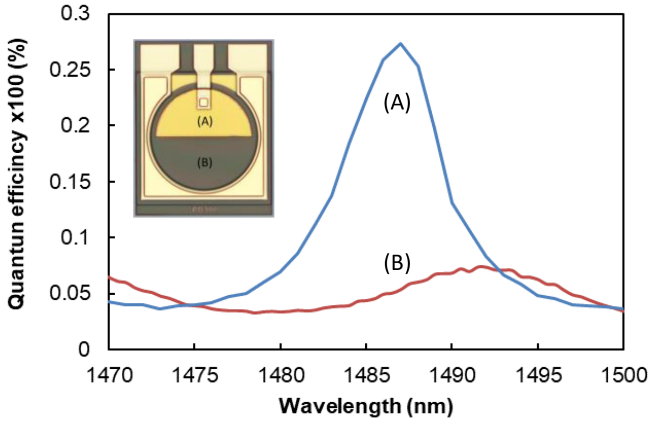

Fig. 6. Measured spectral quantum efficiency of 300 μm large PD covered by (A) Ti/Pt/Au end mirror and (B) polyimide film.

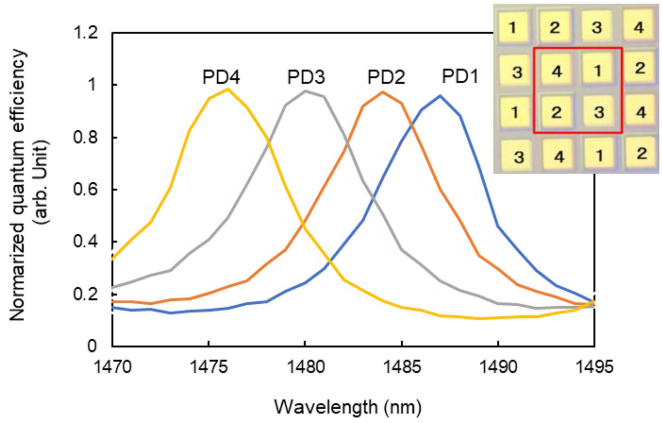

Fig. 7. Measured spectral quantum efficiency of 4λ-PDs (PD1, PD2, PD3 and PD4) in 4 × 4 PD array.

forming four different cavity lengths in PD array, high mesa structure in each PD was fabricated by a dry etching process down to n-InP layer. The n-InP layer was a common electrode for all PD pixels. After making contact hole on isolation film, Au wiring process was employed (see Fig. 5(b)).

B. Responsivity Measurement

We measured the optical resonant characteristic and compared the quantum efficiency (spectral responsivity) in two different regions in a large single PD. As shown in Fig. 6, a 300 μm large diameter single PD contained two different kinds of resonant conditions. Here, condition-A: the half of the 300 μm diameter was covered by the p-top metal to enhance the resonant effect, condition-B: another half of the 300 μm diameter was not covered by p-top metal, but coated by the 2 μm thick polyimide film (refractive index is near 1.6), which would allow low reflectance less than 10%. Although the responsivity of condition-B exhibited the low efficiency (7%), which was comparable to a quantum efficiency calculated from 0.1 μm thin absorption layer without resonance, four times higher efficiency was recognized from condition-A, caused by the resonant effect in the cavity. The high efficiency could be obtained in wavelength range of 1470–1500 nm, which was approximately 50 nm shifted from our target wavelength region (C-band). It could be explained by 5% thinner layer condition against the target layer thickness in multi-stacking DBR growing process.

C. Crosstalk Measurement in 4-WDM Beam

In aim of WDM-FSO communication demonstration, the spectral quantum efficiency was measured for the four different cavity length in PD1, PD2, PD3 and PD4 in 1470–1495 nm (see Fig. 7), where the normalized value of 1 marked in Fig. 7 corresponds to a quantum efficiency of approximately 27%, as seen in Fig. 6. Four similar characteristics can be obtained, as shown in Fig. 7. When the optical beam was irradiated to any four PDs simultaneously in free space, four spectrums could be obtained from each PD. The wavelength distances between the peaks in each PD were varied from 3 nm to 5 nm, which differed from our target (10 nm). We inferred that the difference between them was due to variation on wet etching process. The actual etching rate in 4 × 4 PD array device region located in center part of wafer might be slightly different etching rate in process monitoring region at the edge of wafer.

Following "XT (dB) = 20 × log (I_{PD1}/I_{PD2})", where I_{PD} is photocurrent in each PD, the XT in PD1 photocurrent between PD1 and PD2 was estimated to be −4 dB. The XT between PD1 and PD3 was −11.6 dB, and −18.7 dB between PD1 and PD4 respectively from Fig. 7. From these results, it was supposed that 2-WDM beam direct detection using PD1 and PD4 using 1475 nm and 1487 nm wavelength would be sufficiently possible with low crosstalk (XT(PD1) = −18.7 dB, XT(PD4) = −17.9 dB). When assuming 3-WDM beam direct detection, the three wavelengths of 1475 nm, 1481 nm and 1487 nm were selected for PD1, PD3, and PD4. The XT in each PD under mixing three different wavelength beam condition were estimated to be −8.2 dB in PD1, −2.9 dB in PD3 and −5.3 dB in PD4 respectively. By adjusting the three optical power level, the XT level in each PD channel might be improved more in 3-WDM FSO communication.

D. Frequency Response Measurement

For a WDM-FSO demonstration, a PD array module was designed and fabricated with a metal package. 16 RF coaxial connectors attached to the package side wall were connected to the 16-PD pixels respectively through co-planer waveguide transmission lines using bonding wires. Other passive components including 50 Ω matching resistors and DC blocking capacitors were implemented as well. A small thou-hole was made in center of the large transmission substrate for back-illumination in the PD array device, and then the PD array device was placed on the small thou-hole. Using a lightwave component analyzer, the frequency response was measured for four representative (PD1, PD2, PD3, and PD4) having difference cavity length, where the wavelengths in the range of 1475–1487 nm were prepared to maximize the photocurrent in each of PD1–4. In Fig. 8, a high 3 dB bandwidth in 13–15 GHz with good uniformity in four measurement results could be found.

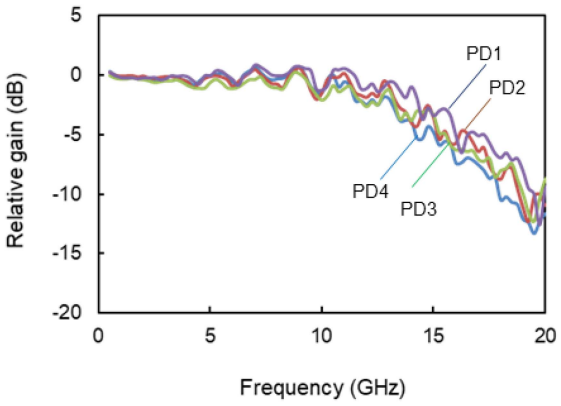

Fig. 8. Frequency response of 4λ-PD pixels in 4 × 4 PD array in 20 GHz range.

These results were not inconsistent with the simulation results discussed in previous section. Comparing the 3 dB bandwidth in the PD array chip, small change of the 3 dB bandwidth in the fabricated PD array module could be seen. It suggested minimum degradations in the PD module implementation process. The 3 dB bandwidth of 13–15 GHz implied a maximum data rate (NRZ) in range of 20–25 Gbps could be expected for a FSO communication demonstration. The ripple beyond 5 GHz was determined to be caused by the S22 RF reflection. Although a good S22 value of <-10 dB could be confirmed at 4 GHz, it degraded to -4 dB at 4–12 GHz owing to a mismatch in the impedance that is composed of 50 Ω resistors and other passive components, including the bonding wire inductance.

IV. WDM-FSO Communication Demonstration

A. Experimental Setup

In the WDM-FSO fundamental demonstration using the fabricated PD array device, three-channel WDM system was built up as shown in Fig. 9, where no beam positioning system including beam tracking and active alignment function were installed not all. The beam size in free space was approximately 1 mm, and the beam size on the PD array surface was inferred to be close to the beam sizes of 2-PD in 2-WDM and 3-PD in 3-WDM. Three wavelengths of 1475 nm, 1481 nm and 1487 nm for PD1, PD3 and PD4 were selected from three S-band laser sources, in order to confirm a proof of our device concept for WDM-FSO communication demonstration. These three laser sources were modulated by three intensity modulators individually though three-channel pulse pattern generator (20–25 Gbps, NRZ). The output power in each intensity modulator was adjusted to the same level, and were combined by an optical coupler. The 2 to 3 WDM signal was amplified by an S-band optical amplifier (+12 dBm) to compensate the low optical input power density in each small PD under the expanded beam condition. After 1.5 m free space transmission, the expanded WDM beam was irradiated to PD1, PD4 simultaneously for 2-WDM-FSO, and PD1, PD3 and PD4 for 3-WDM-FSO. The RF output in each PD was amplified by an RF amplifier, and was analyzed by an oscilloscope and a bit error rate tester.

B. Alignment Tolerance

One of aims in our device concept is enlarging the photodetective area (aperture size) to improve the optical alignment tolerance using the 4 × 4 matrix structure, compared to a single PD. By changing the incident beam position in x-axis on the 15 mm diameter receiver lens, where the beam size was expected to be the same size as that in PD pixel (30 μm), the photocurrent profile from each PD was measured. Fig. 10 shows the measurement results on photocurrent profiles from four PDs (PD1 to PD4) in x-axis, while moving beam position on a receiver lens, where the normalized value = 1 in Fig. 10 corresponds to the quantum efficiency near 27% in Fig. 6. It was found that each PD allowed approximately 1.5–2 mm alignment tolerance in the 15 mm receiver lens. The alignment tolerance on the receiver lens in x-axis in 4 × 4 PD array was estimated to be approximately 7.5 mm from Fig. 10, which indicated a half region on the 15 mm diameter receiver lens.

To realize the simultaneous irradiation of any 2 × 2 PD, the WDM beam is assumed to be aligned with the offset position between 4-PDs arranged with a pitch of 1.5–2.0 mm on the receiver lens, as shown in Fig. 10. Here, an expanded beam (rather than a focused beam) is assumed to irradiate any four (2 × 2) PDs simultaneously, including the PD1–4 in our device concept. It would be difficult for a beam to cover the 2 × 2 PDs and align with them if it is too focused and its size is sufficiently smaller than the gap (excluding the p–n junction area) between the PDs. Moreover, if the beam is sufficiently larger than the 2 × 2 PD area and covers the PDs located outside the 2 × 2 PD, the alignment condition for any four PDs can be preserved. However, the optical power of each PD would be lower, which affects the signal-to-noise ratio. We believe that the optimum beam size is comparable to that of the 2 × 2 PDs.

Moreover, each photocurrent was crossed at near 20% from the peak. It suggested that the photocurrent could be obtained by neighboring pixels at non-sensitive position related to a gap between PDs. The four zigzag photocurrent profile in Fig. 10 will be flatten with a larger beam spot by sacrificing the responsivity. When a 2-λ multiplexed (2-WDM) beam simultaneously irradiates both PD1 and PD3 as shown in the left column of Fig. 5(a) with misalignment in the *y*-axis direction, few crosstalk affections are expected in PD1 and PD3 because of the low crosstalk (-11.6 dB) in PD1 and PD3. The same result can be expected for PD2–PD4 in the second left column of Fig. 5(a). However, the crosstalk affection is more emphasized for a beam with an *x*-axis misalignment, except for the misalignment in PD1–PD4 in the current device. To achieve higher alignment robustness in 3-WDM and 4-WDM, a lower crosstalk between neighboring PDs is required.

C. 2-WDM-FSO Communications

As expected in last measurement section regarding "WDM responsivity in 4 × 4 PDA", 2-WDM communication demonstration using 1475 nm and 1487 nm wavelength would be sufficiently successful under the low crosstalk (in -17 dB range) condition between PD1 and PD4 pixels. When 20 Gbps (NRZ)

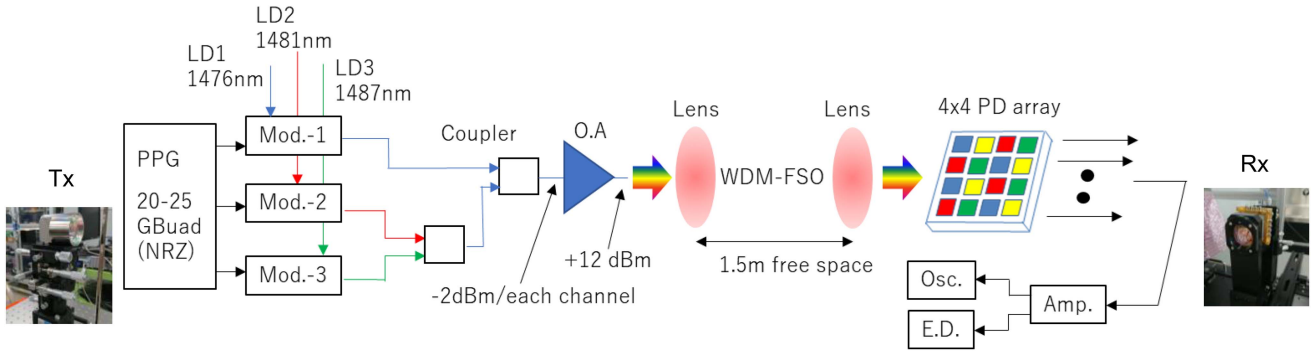

Fig. 9. Experimental setup for WDM FSO communications using resonant cavity PD array device.

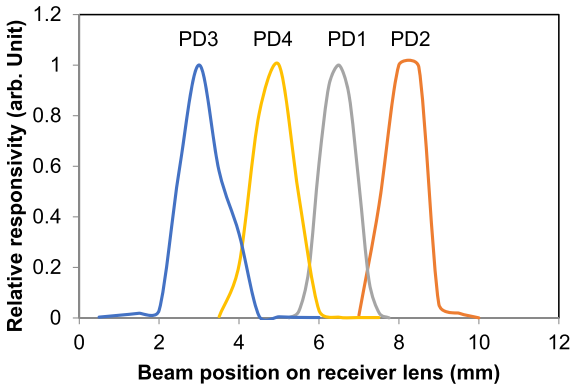

Fig. 10. Photocurrent profiles from four PDs (PD1 to PD4) in x-axis while moving position on receiver lens.

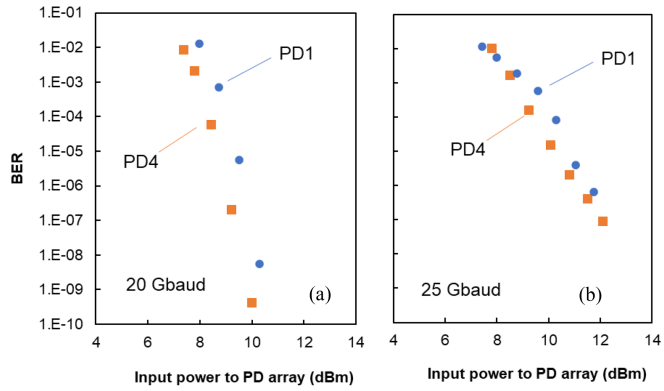

Fig. 12. BER measurement results on PD1 and PD4 at (a) 20 Gbps and (b) 25 Gbps in 2-WDM FSO communication demonstration.

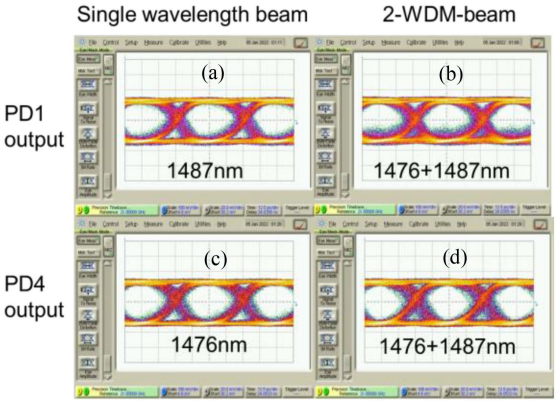

Fig. 11. Eye diagrams, (a) 1475 nm single beam detection in PD1, (b) 1475 nm and 1487 nm WDM beam simultaneous detection in PD1, (c) 1487 nm single beam detection in PD4, (d) 1475 nm and 1487 nm WDM beam simultaneous detection in PD4.

2-WDM beam was irradiated to both PD1 and PD4 simultaneously, the eye diagrams in each PD were evaluated. Fig. 11 shows the eye diagrams for (a) 1475 nm single beam detection and (b) 1475 nm and 1487 nm WDM beam simultaneous detection in PD1, and for (c) 1487 nm single beam detection and (d) 1475 nm and 1487 nm WDM beam simultaneous detection in PD4. Comparing the eye diagrams in (a) and (b), or in (c) and (d), very few crosstalk affections were recognized in 2-WDM detection from those eye diagrams, even though some noises in zero-level in (b) or jitter in falling point in (d) were added due to crosstalk. Clear eye openings in (b) and (d) could be observed.

Fig. 12 shows a measurement result on bit error rate (BER) for 2-WDM beam detection in both PD1 and PD4 at 20 Gbps and 25 Gbps. In the straightforward BER curves at 20 Gbps in Fig. 12(a), the similar BER performance could be observed in PD1 and PD4. We found the good characteristics on BER $=$ 10^{-9}–10^{-10} at $+10$ dBm, and a small difference of the receive power (0.5 dB) between them in BER range of 1×10^{-3} to 1×10^{-8}. Even though the steep BER lines at 20 Gbps was changed to be shallow at 25 Gbps (see Fig. 12(b)), it could be obtained in BER $= 10^{-5}$ range at $+10$ dBm. The high power of $+10$ dBm is related to the offset beam position between the PDs in order to provide simultaneous irradiation to several PDs. This might be improved by optimizing the PD pixel layout and introducing a higher gain RF amplifier than 20 dB.

Next, we investigated inter-crosstalk affection in BER in each PD through the 2-WDM FSO demonstration. Comparing the BER curve under two kind of beam conditions (the single beam and 2-WDM beam), the crosstalk penalty was estimated as shown in Fig. 13. At 20 Gbps, the received power to 1475 nm single beam was 8 dBm at BER $= 1 \times 10^{-8}$, and then approximately 2 dB difference between those two conditions in above was found in PD1 (see Fig. 13(a)). Moreover, the same penalty of approximately 2 dB in 2-WDM beam was recognized

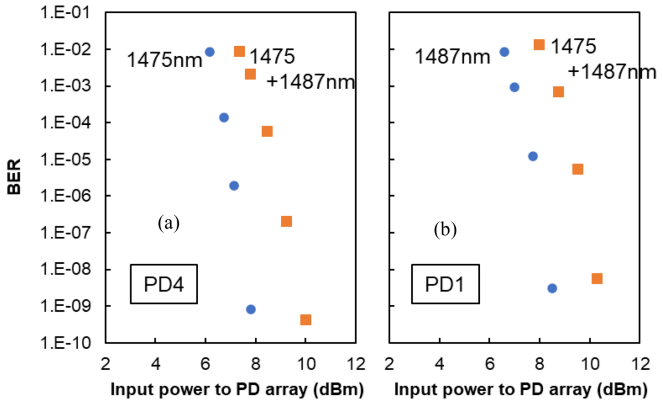

Fig. 13. BER curve on crosstalk penalty at 20 Gbps for (a) PD4 and (b) PD1 using single beam and 2-WDM-beam.

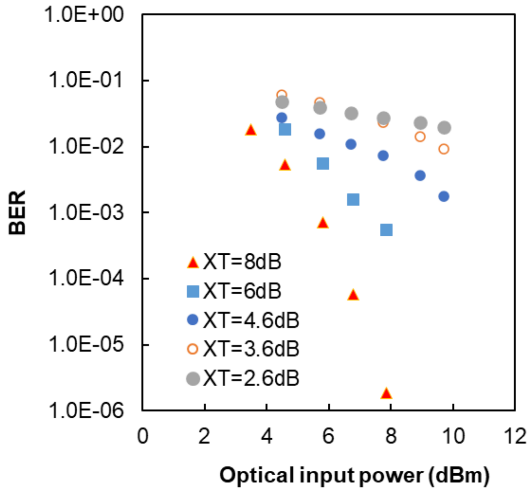

Fig. 14. Fundamental BER characteristic on PD4 in 4 × 4 PD array device by changing XT level.

against that in 1487 nm single beam detection in PD4 as well (see Fig. 13(b)). Therefore, the 2 dB inter-cross affection was included in the resonant cavity PD array device in the 20 Gbps 2-WDM FSO communication demonstration.

D. 3-WDM-FSO Communications

Before 3-WDM-FSO communication demonstration, we discussed about the expected BER with respect to the crosstalk (XT) affection using two PDs (PD1, PD4). Here, the BER was measured by changing the optical power ratio between two PDs (PD1:1487 nm, PD4:1475 nm) to enhance the crosstalk. The mixed two optical signals at 20 Gbps was focused to the only PD4 in the XT range from −8 dB to −2.6 dB, and then the BER was measured with the increase of the total optical power up to +10 dBm as shown in Fig. 14. Below XT = −6 dB, the straightforward steep BER curve could be seen, and was changed to be flatten above XT = −6 dB. To satisfy BER = 3.8×10^{-3} in consideration of 7% FEC limit, a lower XT than −4.6 dB was required in +10 dBm range. In 20% FEC limit, a minimum crosstalk of −2.6 dB would be needed to satisfy BER = 2×10^{-2}. When assuming 3-WDM beam detection using PD1, PD3, PD4 excluding PD2 (λ = 1479 nm), the crosstalk in each PD were estimated to be −8.2 dB in PD1, −2.9 dB in PD3 and −5.3 dB in PD4 outputs respectively. These results satisfied the BER lower than 2×10^{-2} resulting from Fig. 14.

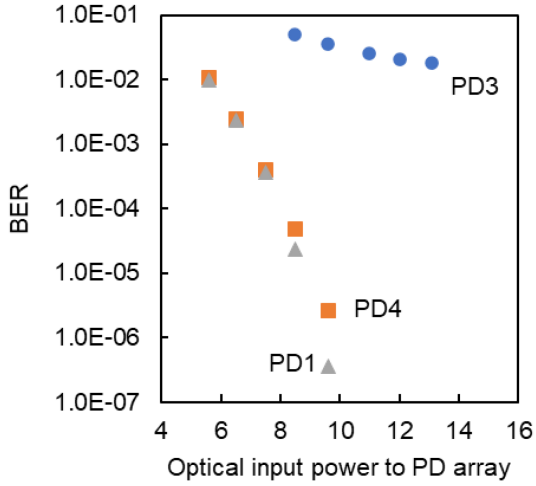

Fig. 15. BER measurement results on PD1, PD3 and PD4 in 3-WDM FSO communication demonstration at 20 Gbps × 3 (60 Gbps).

Next, 3-WDM-FSO communication demonstration was carried out at 20 Gbps (60 Gbps) using three PDs (PD1, PD3, PD4). Reducing the crosstalk of −5.3 dB in PD4 less than −6 dB, optical input power level to PD3 was slightly adjusted to 0.5–1 dB lower than original power condition. It should be effective to preserve lower XT in PD4 than −5.3 dB. Fig. 15 shows the measurement results of BERs for PD1, PD3, PD4 in a 3-WDM mixed beam. Good BER curves from PD1 and PD4 could be obtained with lower BER than 1×10^{-3}. The flatten BER curve was seen from PD3 due to larger XT than −2.9 dB. However, we confirmed the XT less than 2×10^{-2}, which was in good agreement with the discussion in above from Fig. 14. Therefore, 3-WDM FSO beam at 20 Gbps (60 Gbps = 20 Gbps × 3) could be successfully received by three resonant cavity PDs in 4 × 4 PD array with BER less than 2×10^{-2}.

We can inductively infer the BER performance with respect to the misalignment based on the results shown in Fig. 14. For example, when considering y-axis misalignment in 2-WDM, a good BER of less than 1×10^{-6} can be expected because a crosstalk of approximately −11.6 dB between PD1 and PD3 was obtained. However, *x*-axis misalignment, except for that in PD1–PD4, leads to poor BER results because of the enhancement of the crosstalk in PD1–PD2, PD2–PD3, and PD3–PD4. When assuming a crosstalk of −4 dB for example, as obtained in Section III-C, a BER approximately in the 10^{-2} range is obtained as the best case. If the PD array device described in Section II (device design) can be realized, higher optical alignment robustness can be achieved against the BER (crosstalk).

The large crosstalk between adjacent channels could be attributed to the narrow wavelength pitch of 3–5 nm between the four peaks. When the four-wavelength pitch was adjusted to 10 nm (target), the crosstalk was approximately −15 dB.

Another option to improve the crosstalk is to increase the finesse factor by using front and end mirrors of higher reflectance, which sharpens the broad peak profile.

V. Conclusion

We fabricated the resonant cavity type high speed 4 × 4 PD array device for WDM-FSO communication, which enable both WDM-FSO beam direct coupling excluding an AWG and higher optical alignment robustness at the same time. Although four different cavity length and DBR mirror in 4 × 4 PD array were carefully fabricated by etching process and epitaxial multi-stacking process. Four different peak profiles with approximately 5 nm pitch in spectral responsivity could be found in the fabricated device for 4WDM-FSO communications. For the WDM-FSO communication demonstration, the 4 × 4 PD array module was fabricated and could work well with approximately 15 GHz bandwidth. Thanks to the large aperture size (162 μm × 162 μm) 4 × 4 PD array device, a high optical alignment robustness could be achieved in 7 mm alignment tolerance on receiver lens in 1.5 m free space. In consideration of the crosstalk between PDs, 2-WDM FSO communication at up to 25 Gbps per channel was successfully demonstrated. In addition, the PD array device has a potential to receive 3-WDM-FSO beam with BER $< 2 \times 10^{-2}$, from both crosstalk analysis and experimental results. The 4-WDM FSO communications at 25 Gbps (25 Gbps × 4) will be achieved by correcting the fabrication process to reduce the crosstalk in the spectrum responsivity. To scale up the number of multiplexed wavelengths in the C-band (or in the 40 nm wavelength region), the finesse factor (or full width at half maximum wavelength, FWHM) is taken into account. By increasing the finesse factor (i.e., a narrow FWHM) in each resonant peak using a high-reflectance front (98%) and end (100%) mirrors with the optimized cavity length difference between PDs, a scale-up of approximately 16-wavelengths with −18 dB crosstalk can be achieved, where the cavity length (L) and absorption layer thickness (d) were assumed constant in the current design, as shown in Fig. 2. However, a narrow FWHM of approximately 3 nm is required to extend the wavelength numbers, as opposed to a wide FWHM of 18 nm in the current design. The proposed device will be applicable not only for compact WDM-FSO communication applications, but also might be useful for pluggable ethernet transceivers applications and Vertical Cavity Surface Emitting LASER (VCSEL) NxN array based short distance communications.

Acknowledgment

We thank Mr. Nakajima and all technical staffs in the photonic device laboratory in NICT for supporting the fabrication process.

References

[1] Huawei White Paper: 5G Network Architecture -A High-Level Perspective, 2016. [Online]. Available: https://www-file.huawei.com/-/media/corporate/pdf/mbb/5g_nework_architecture_whitepaper_en.pdf?la=en

[2] M. G. L. Frecassetti et al., "D-band radio solutions for beyond 5G reconfigurable meshed cellular networks," in *Proc. 16th Int. Symp. Wireless Commun. Syst.*, 2019, pp. 427–431.

[3] N. A. M. Nor, I. M. Rafiqul, W. Al-Khateeb, and S. A. Zabidi, "Environmental effects on free space earth-tosatellite optical link based on measurement data in Malaysia," in *Proc. Int. Conf. Comput. Commun. Eng.*, 2012, pp. 694–699.

[4] NTT DoCoMo, White Paper 5G Evolution and 6G, Jan. 2020. [Online]. Available: https://www.nttdocomo.co.jp/english/binary/pdf/corporate/technology/whitepaper_6g/DOCOMO_6G_White_PaperEN_20200124.pdf

[5] E. Ciaramella et al., "1.28 Terabit/s (32×40 Gbit/s) WDM transmission over a double-pass free space optical link," in *Proc. Conf. Opt. Fiber Commun.*, 2009, Paper OMN7.

[6] K. Matsuda et al., "Demonstration of a real-time 14 Tb/s multi-aperture transmit single-aperture receive FSO system with class 1 eye-safe transmit intensity," *J. Lightw. Technol.*, vol. 40, no. 5, pp. 1494–1501, Mar. 2022.

[7] G. Parca, A. Shahpari, V. Carrozzo, G. M. Tosi Beleffi, and A. L. J. Teixeira, "Broadband free space optical urban links for next generation infrastructures and services," in *Proc. 15th Int. Conf. Transparent Opt. Netw.*, 2013, Paper Tu.B3.2.

[8] E. Erdogan, I. Altunbas, G. K. Kurt, M. Bellemare, G. Lamontagne, and H. Yanikomeroglu, "Site diversity in downlink optical satellite networks through ground station selection," *IEEE Access*, vol. 9, pp. 31179–31190, 2021.

[9] T. Koonen, J. Oh, K. Mekonnen, Z. Cao, and E. Tangdiongga, "Ultra-high capacity indoor optical wireless communication using 2D-steered pencil beams," *J. Lightw. Technol.*, vol. 34, no. 20, pp. 4802–4809, Oct. 2016.

[10] H. Haas et al., " Introduction to indoor networking concepts and challenges in LiFi," *J. Opt. Commun. Netw.*, vol. 12, no. 2, pp. A190–A203, Feb. 2020.

[11] R. K. Sharma, H. Kaushal, and P. K. Sharma, "Analysis of indoor FSO link under diffused channel topology," in *Proc. Int. Conf. Comput. Commun. Automat.*, 2015, pp. 1286–1272.

[12] S. Muta, T. Tsujimura, and K. Izumi, "Laser beam tracking system for active free-space optical communication," in *Proc. IEEE/SICE Int. Symp. Syst. Integration*, 2013, pp. 879–884.

[13] A. Bekkali, H. Fujita, and M. Hattori, "Fiber-to-fiber FSO system with advanced VCM controlled laser beam pointing and tracking," in *Proc. Opt. Fiber Commun. Conf. Exhib.*, 2021, Paper W7E.6.

[14] S. S. Murtaza, H. Nie, J. C. Campbell, J. C. Bean, and L. J. Peticolas, "Short-wavelength, high-speed, Si-based resonant-cavity photodetector," *IEEE Photon. Technol. Lett.*, vol. 8, no. 7, pp. 927–929, Jul. 1996.

[15] G. Sen, B. Mukhopadhyay, and P. K. Basu, "Ge/SiGe RCE photodetectors: A comparative study based on Franz-Keldysh effect and quantum confined stark effect," in *Proc. Int. Conf. Comput. Devices Commun.*, 2009, pp. 1–4.

[16] I.-H. Tan et al., "High quantum efficiency and narrow absorption bandwidth of the wafer-fused resonant In0.53Ga0.47As photodetectors," *IEEE Photon. Technol. Lett.*, vol. 6, no. 7, pp. 811–813, Jul. 1994.

[17] S. Ghosh, B. Mukhopadhyay, and G.-E. Chang, "Design and analysis of GeSn-based resonant-cavity-enhanced photodetectors for optical communication applications," *IEEE Sensors J.*, vol. 20, no. 14, pp. 7801–7809, Jul. 2020.

[18] E. Ozbay, I. Kimukin, N. Biyikli, and G. Tuttle, "High-speed GaAs-based resonant-cavity-enhanced 1.3-μm photodetector," *Proc. SPIE*, vol. 3948, Apr. 2000, pp. 170–178 .

[19] K. Kishino, M. S. Unlii, J.-I. Chyi, J. Reed, L. Arsenault, and H. Morkoq, "Resonant cavity -enhanced (RCE) photodetectors," *IEEE J. Quantum Electron.*, vol. 21, no. 8, pp. 2025–2034, Aug. 1991.

[20] M. S. Unlu and S. Strite, "Resonant cavity enhanced photonic devices," *J. Appl. Phys.*, vol. 78, no. 2, pp. 607–639, Jul. 1995.

[21] T. Umezawa, T. Sakamoto, A. Kanno, N. Yamamoto, and T. Kawanishi, "High speed 2-D photodetector array for space and mode division multiplexing fiber communications," *J. Lightw. Technol.*, vol. 36, no. 17, pp. 3684–3692, Sep. 2018.

[22] K. Kusakata, T. Umezawa, N. Yamamoto, and T. Kawanishi, "Improvement of crosstalk of highspeed 2D photodetector array," *Proc. SPIE*, vol. 10945, Feb. 2019, Art. no. 109450O.

[23] T. Umezawa et al., "400-Gbps space division multiplexing optical wireless communication using two-dimensional photodetector array," in *Proc. Eur. Conf. Opt. Commun.*, 2018, Paper Th2.31.

[24] Y. Yoshida, T. Umezawa, A. Kanno, and N. Yamamoto, "A phase retrieving coherent receiver based on two-dimensional photodetector array," *J. Lightw. Technol.*, vol. 38, no. 1, pp. 90–100, Jan. 2020.

[25] T. Umezawa et al., "FSO receiver with high optical alignment robustness using high-speed 2D-PDA and space diversity technique," *J. Lightw. Technol.*, vol. 39, no. 4, pp. 1040–1047, Feb. 2021.

[26] T. Umezawa et al., "25-Gbaud 4-WDM free-space optical communication using 32-pixel high-speed 2D photodetector array," *J. Lightw. Technol.*, vol. 37, no. 2, pp. 612–618, Jan. 2019.

Toshimasa Umezawa received the B.E. and M.E. degrees in electronics from the Nagaoka University of Technology, Niigata, Japan, in 1984 and 1986, respectively, and the Ph.D. degree in electronics from Tokyo University, Tokyo, Japan, in 1995. From 1987 to 2011, he was with Yokogawa Electric Corporation. He was also with Central Research Laboratory and Photonics Business Department. In 1992, he was a Visiting Scholar with the Department of Applied Physics, Stanford University, Stanford, CA, USA. He was engaged in research on superconductor devices, photonics devices, and their applications with Tokyo University. In 2011, he joined the National Institute of Information and Communications Technology, Tokyo. He is a Member of the Institute of Electronics, Information, and Communication Engineers, Japan Society of Applied Physics. His research interests include E/O devices and photonic integrated circuits and millimeter-wave photonics.

Shoichi Takamizawa received the B.E. and M.E. degrees from the Department of Electronic and Physical Systems, School of Fundamental Science and Engineering, Waseda University, Tokyo, Japan, in 2019 and 2021, respectively. In 2020, he was the recipient of the Best Presentation Award in OECC 2020. Since 2022, he has been with Fuji Technical Research Corporation. His research interests include semiconductor devices and photonic integrated circuits.

Atsushi Matsumoto (Member, IEEE) received the B.S. degree in electronics, information, and communication engineering in 2003, and the M.S. and Dr. Eng. degrees in electrical engineering and bioscience from Waseda University, Tokyo, Japan, in 2005 and 2015, respectively. He is currently a Senior Researcher of the National Institute of Information and Communications Technology, Tokyo. He is a Member of the Japan Society of Applied Physics, and Institute of Electronics, Information and Communication Engineers of Japan.

Kouichi Akahane received the B.E., M.E., and Ph.D. degrees in materials science from the University of Tsukuba, Tsukuba, Japan, in 1997, 1999, and 2002, respectively. In 2002, he joined Communications Research Laboratory (from April 1, 2004, National Institute of Information and Communications Technology), Koganei, Tokyo. He is currently the Director of Optical Access Technology Laboratory, National Institute of Information and Communications Technology and is currently working on semiconductor photonic devices.

Naokatsu Yamamoto received the Ph.D. degree in electrical engineering from Tokyo Denki University, Tokyo, Japan, in 2000. In April 2001, he joined the National Institute of Information and Communications Technology (NICT). He also joined Tokyo Denki University as a Visiting Professor in May 2008 and the Ministry of Internal Affairs and Communications as the Deputy Director from July 2012 to September 2013. Since 2020, he has been an Associate Director General of Photonic ICT Center, NICT, and also has been the Director of Advanced ICT Device Laboratory. His research interests include heterogeneous quantum dot laser with silicon photonics, and a convergence device technology of photonics and wireless. Recently, he has also interested in the use of a 1.0-μm waveband (thousand-band, T-band) as a new optical frequency band for short-range communications.

Atsushi Kanno (Senior Member, IEEE) received the B.Sc., M.Sc., and Ph.D. degrees in science from the University of Tsukuba, Japan, in 1999, 2001, and 2005, respectively. In 2005, he was with the Venture Business Laboratory, Institute of Science and Engineering, University of Tsukuba. In 2006, he joined the National Institute of Information and Communications Technology, Japan. Since August 2022, he has been with the Nagoya Institute of Technology, Japan. His research interests include microwave photonics and broadband optical and radio communication systems and their sensing applications. He is a Member of the Institute of Electronics, Information and Communication Engineers, Japan Society of Applied Physics, Laser Society of Japan, and SPIE.

Tetsuya Kawanishi (Fellow, IEEE) received the B.E., M.E., and Ph.D. degrees in electronics from Kyoto University, Kyoto, Japan, in 1992, 1994, and 1997, respectively. From 1994 to 1995, he was with Production Engineering Laboratory, Panasonic. In 1997, he was with Venture Business Laboratory, Kyoto University, where he was involved in research on electromagnetic scattering and near-field optics. In 1998, he joined the Communications Research Laboratory, Ministry of Posts and Telecommunications (now the National Institute of Information and Communications Technology), Tokyo, Japan, where he is currently a Research Executive Director. In 2004, he was a Visiting Scholar with the Department of Electrical and Computer Engineering, University of California at San Diego, La Jolla, CA, USA. In 2015, he joined the Department of Electronic and Physical Systems, Waseda University, Tokyo, as a Professor. His research interests include high-speed optical modulators and RF photonics.